Journal of Radioanalytical and Nuclear Chemistry (2020) 324:1351–1364
https://doi.org/10.1007/s10967-020-07167-9

The use of titanium oxide/polyethylene glycol nanocomposite in sorption of ^{134}Cs and ^{60}Co radionuclides from aqueous solutions

G. A. Dakroury[1] · Sh. F. Abo-Zahra[1]

Received: 21 February 2020 / Published online: 4 May 2020

Abstract
Titanium dioxide/polyethylene glycol (TiO_2/PEG PNC)-nanocomposite was prepared using the wet chemical method. Physico-chemical characterization of TiO_2/PEG PNC is studied by TEM, FTIR, XRD, DTA-TGA, particle size distribution, and pore size analysis. TiO_2/PEG PNC used for sorption of ^{134}Cs and ^{60}Co radionuclides. The TiO_2/PEG PNC sorption monolayer capacities towards ^{134}Cs and ^{60}Co radionuclides at pH 5 and 25 °C is numerically equal to 163.28 ± 10.98, and 330.16 ± 41.60 mg g^{-1}, respectively. The kinetic of the sorption reaction is applicable with a pseudo-second-order model. The sorption reaction is favorable and endothermic.

Keywords Titanium dioxide · Nanocomposite · Sorption · Radioactive waste

Introduction

Nano-sized materials are a new solid that takes a large portion of attention in recent years due to its special properties (such as small size (1–100 nm), numerous specific surface area [1–3]. Thus, the nano-materials are able to provide a selective high sorption capacity towards trace mineral ions.

A previous study showed that TiO_2 nanoparticles could adsorb heavy metal ions [4] and rare earth elements [5]. The disadvantage in using nanometal oxides as a sorbent is the agglomeration due to van der Waals interactions [6] as a result for the increase in surface area, which makes metal oxide particles unstable. Thus, the metal oxide may lose selectivity, mechanical strength, and high adsorption capacity. To overcome this disadvantage, polymeric supports, with a large surface area, adjustable surface chemistry, perfect mechanical hardness, and pore size distribution, could be used for metal oxides immobilization [6, 7].

Polyethylene glycol (PEG) is a hydrophilic polymer capable of creating a uniform surface, smooth coating and well-defined particles [8], as it reduces cracked surface formation in the immobilizer system [9]. Most reports on nano TiO_2 immobilized with PEG have been identified to enhance photosynthesis due to porosity effect and greater specific surface area [10, 11]. Trapalis et al. [12] found that as the weight percent of PEG introduced in the TiO_2 film increases, the porosity consequently increases. However, no detailed study was conducted on the sorption behavior of TiO_2 immobilized with PEG towards radioactive waste.

A large amount of radioactive wastewater has been produced in conjunction with the advances in nuclear industry. ^{90}Sr, ^{134}Cs, and ^{60}Co are the most important radionuclides in low-level aqueous wastes in terms of a possible dose of humans [13–15]. Adsorption of radionuclides from their solutions is one of the various steps used in the treatment of radioactive liquid-waste using suitable adsorbent, (activated and impregnated carbon, clays, alumina silicates, organic, and inorganic gels and others, have been reported) [16–22].

Therefore, this work aims to prepare TiO_2/PEG PNC and explain the physicochemical characteristics using FTIR, TEM, X-ray diffraction, DTA-TG, particle size distribution, and pore size analysis. The sorption of ^{134}Cs and ^{60}Co on TiO_2/PEG PNC is studied. Optimization of the reaction conditions such as (pH, shaking time, sorbent concentration, and temperature have been investigated. Moreover, the specifications of the sorption reaction as kinetics mechanism, isotherms models, and thermodynamic parameters are studied.

✉ G. A. Dakroury
dr_gdakrory2010@yahoo.com

[1] Nuclear Chemistry Department, Hot Laboratories Centre, Atomic Energy Authority, P.O. 13759, Cairo, Egypt

Experimental

Chemicals

All chemicals used were of (AR) and were used without additional purification. Titanium tetra isopropyl orthotitanate ($C_{12}H_{28}O_4Ti \geq 97\%$) obtained from Merck Germany, Isopropyl alcohol ($C_3H_8OH \geq 99.7\%$) obtained from Prolabo, England. Ammonium hydroxide (NH_4OH) 33% from Edwic El-Nasr, Egypt. Polyethylene glycol 1500, H $(OCH_2CH_2)_n$ OH Extra Pure Obtained from Kosdaq. China. Dehydrated alcohol, absolute ethanol C_2H_5OH, 99.9% obtained from International Company for Sup. & MED. Industries, Egypt.

Hydrochloric acid (HCl) and sodium hydroxide (NaOH) were obtained from El-Nasr Co. (ADWIC), Egypt, used to adjust the pH of the solutions. Cesium chloride (CsCl) and cobalt chloride ($CoCl_2$) were purchased from Merck, (Germany). For all experiments, (DDW) double-distilled water was used for the preparation of solutions.

The radionuclides of two elements (^{134}Cs and ^{60}Co) were produced by irradiation of cesium chloride and cobalt chloride powders in the Second Egyptian Research Reactor (ET-RR-2). The initial activity were 42.2 KBq/L, and 14.3 KBq/L for ^{134}Cs and ^{60}Co radionuclides respectively.

A stock solution of (^{134}Cs and ^{60}Co) were prepared by dissolving a certain amount of cesium and cobalt salts in double-distilled water and spiked with the ^{134}Cs and ^{60}Co radionuclides. These solutions were kept as stock radioactive solutions for all experiments.

Preparation of nano-sized TiO_2 powder (TiO_2 NPs)

Nano-sized TiO_2 is prepared by the sol–gel hydrolysis technique using titanium tetra isopropyl orthotitanate as a precursor. The preparation technique includes the hydrolysis of alkoxide (tetra isopropyl orthotitanate) to form sol and then the gel phase is formed after polymerization of sol using a catalyst [23]. The flow chart in Fig. 1a summarizes the steps for TiO_2 NPs preparation.

Preparation of TiO_2/PEG nanocomposite (TiO_2/PEG PNC)

The 1:1 PEG/TiO_2 nanocomposite was prepared using a wet chemical technique [24] where PEG was adsorbed on the TiO_2 surface. 5 g of polyethylene glycol in 20 ml ethanol and added drop wisely to a solution of 5 g of the calcined nano-TiO_2 powder. The mixture was lied in ultrasonic for 10 min. The whole mixture was stirred for 3hours. The gelatin was dried at 80 °C for 48 h. The flow chart in Fig. 1b summarizes the steps for TiO_2/PEG PNC preparation.

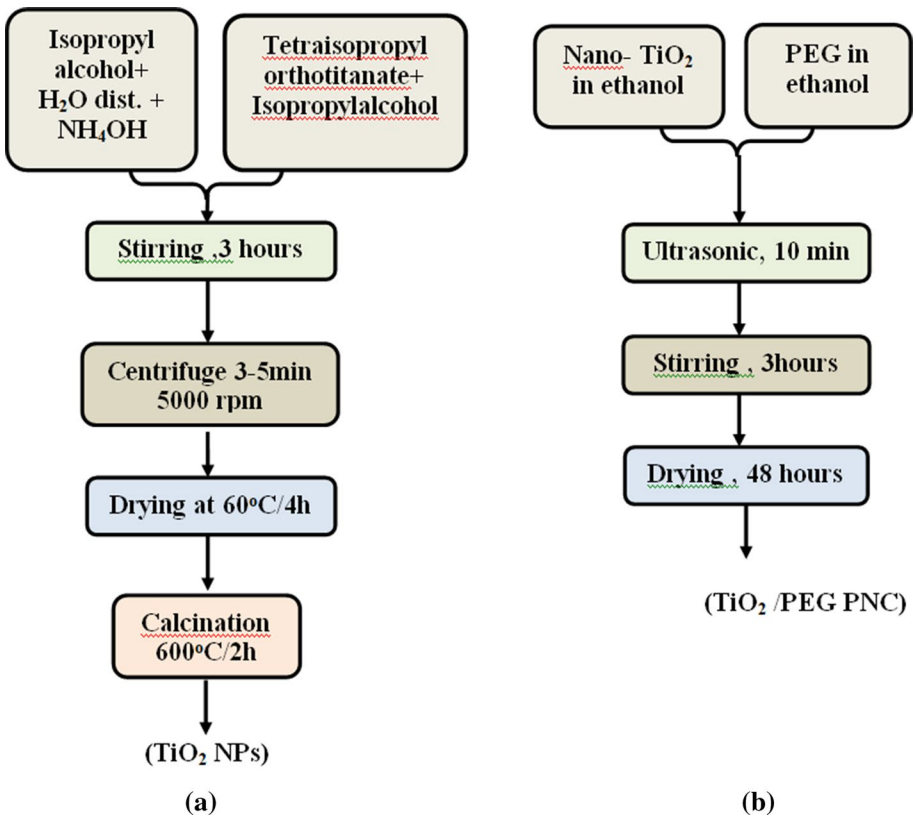

Fig. 1 Flow chart for preparation of **a** TiO_2 NPs and **b** TiO_2/PEG PNC

Instruments and apparatus

The scanning electron microscope (SEM) combined with energy-dispersive X-ray spectroscopy and electron backscatter diffraction (SEM, FEI Quanta FEG-250, and EDX). The transmission electron micrograph image (TEM), for the particle size was recorded on a TEM, JEM2100, and Jeol.s.b, Japan. The X-ray diffraction (XRD) in a Philips X'PERT multipurpose X-ray diffractometer with copper emission lines. Thermal properties of the samples studied using thermo gravimetric analysis (TGA) performed on a Perkin Elmer TGA6 instrument. The sample was heated from 298 to 973 K with a heating rate of 283 K/min under a nitrogen atmosphere with a flow rate of 20 mL/min. Fourier transform infrared (FT-IR) spectra of the samples were recorded using an IR spectrometer with Fourier transformation (Thermo Nicolet Nexus FT-IR, Waltham, MA, USA. The particle size of the prepared samples determined using Zetasizer Nano-Zs, MALVERN, UK. Pore size distribution and corresponding porosity of the prepared powders investigated applying mercury intrusion porosimetry technique with the aid of Pore-sizer chromatech 9320, USA. The activity of radionuclides have been measured radiometrically by high resolution (7.5%) NaI (Tl) detector model 802-3X3, Canberra, USA.

Sorption batch studies

0.05 g of the TiO_2/PEG PNC with (100 mg L^{-1}) of the solution labeled with ^{134}Cs and ^{60}Co radionuclides at various time range (1–120 min), temperatures 25 °C, 40 °C, and 60 °C, and optimum pH. The activity of both radionuclides was determined and the amount of radionuclides, q_t (mg g^{-1}), was calculated from the following equation:

$$q_t = \frac{A_0 - A_t}{A_0} x C_0 x \frac{V}{m} \quad (1)$$

where (A_o and A_t) are the activity of the solution at initial and any time t, respectively, (C_o) is the initial concentration of ions, (V) is the volume of the solution (10 mL), and (m) is the weight of adsorbent (0.05 g).

Sorption isotherm studies

Sorption isotherm studies of ^{134}Cs and ^{60}Co radionuclides [25] were investigated at different concentrations (50–300 mg L^{-1}) onto the prepared materials by adding a certain weight of the sorbent (0.05) to solution of ions labeled by the radionuclides for 30 min. The pH value of the solution was adjusted at (5 ± 0.1). Different isotherm models such as Langmuir and Freundlich isotherm models were studied.

Results and Discussion

Characterization of the prepared nanocompositel

SEM and TEM measurement

Figure 2a represents the dispersion of TiO_2 and PEG in TiO_2/PEG PNC. There is neither phase separation nor cracking in the prepared composite but a rough and fractured surface is obtained [24, 26]. The white nanoparticles are constituted of TiO_2 NPs and the dark surrounding area is constituted of the organic matrix of PEG.

Figure 2b shows a TEM analysis of TiO_2/PEG PNC with a significant presence of nanoparticles reveals [27]. The obtained image is mostly composed of aggregates of hexagonal and irregular particles with a particle size below 20 nm. The aggregation attributes to the sol–gel preparation method.

Particle size statistics and porosity

The particle size statistics is represented in Fig. 3. The sample were ground in the mill and dispersed ultrasonically in non polar solventand water for TiO_2/PEG PNC and TiO_2 NP, respectively.

The nanocharacter appears in TiO_2 particles while; the particle size distribution varies between nano-size to fine for TiO_2/PEG PNC. The increase in particle size is due to the chemical adsorption of PEG molecules onto TiO_2 [28].

The porosity and pore parameters of TiO_2/PEG PNC were illustrated in Table 1. The porous structure of TiO_2/PEG PNC is clarified as the porosity is 32.78%, TiO_2/PEG PNC porosity strongly depends on the amount and molecular weight of PEG [12, 29].

FT-IR analysis

Figure 4a, b shows a sequence of FT-IR spectra for TiO_2 NPs and TiO_2/PEG PNC respectively. Figure 4a represents the spectrum of TiO_2 NPs, clearly shows bands at 3862 cm^{-1}, 2979 and 2901 cm^{-1}, assigned to the stretching vibration of the hydroxyl group O–H of the TiO_2 NPs. The presence of the O–H group belongs to the remaining water/humidity molecules in the crystals lattice of the TiO_2 sample. The band observed around 1633 cm^{-1}, corresponding to bending modes of water Ti–OH; a strong noticeable peak at 1051 cm^{-1} related to Ti–O modes [30, 31].

The FT-IR spectrum of TiO_2/PEG PNC is given in Fig. 4b, a considerable change represents in the spectrum

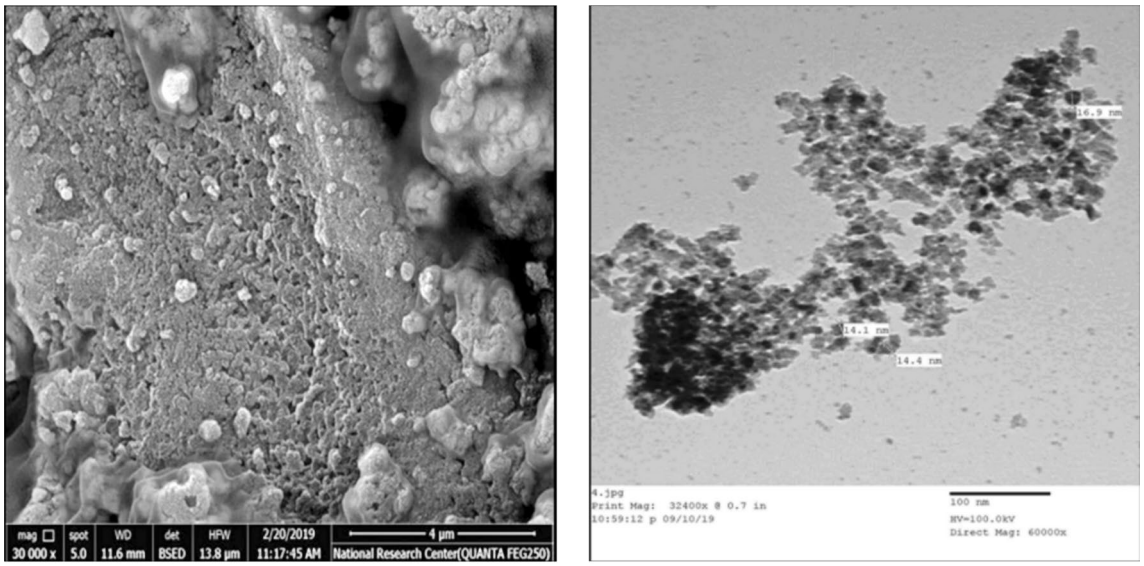

(a) **(b)**

Fig. 2 **a** SEM and **b** TEM image of TiO_2/PEG PNC

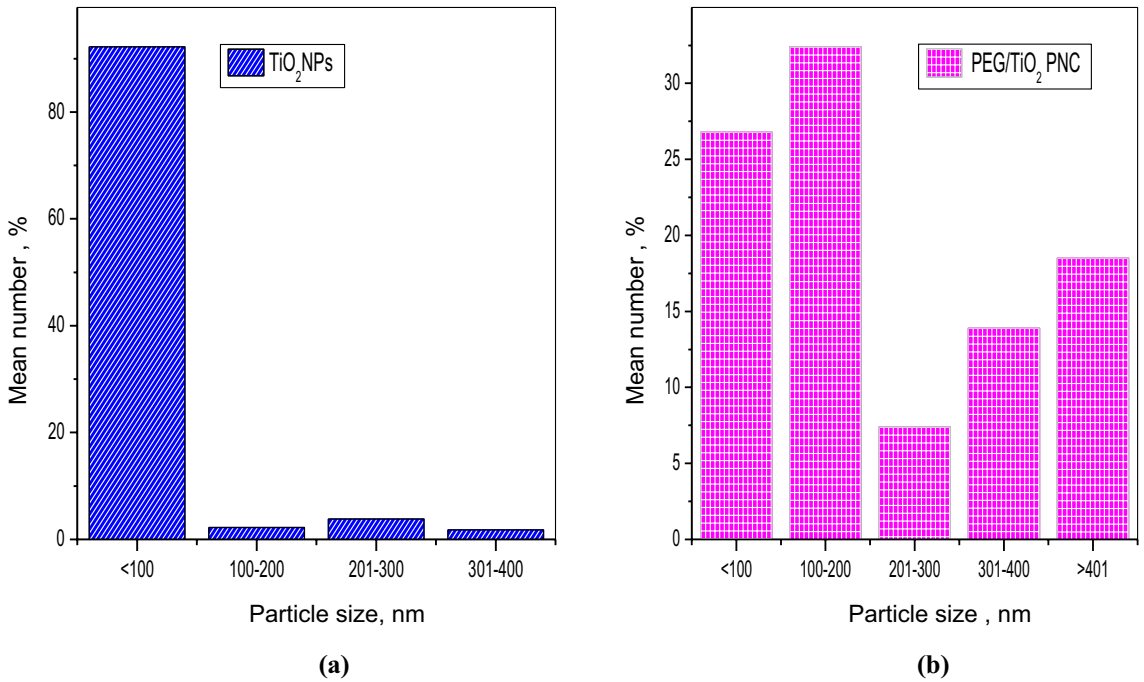

(a) **(b)**

Fig. 3 Particle size distribution of **a** TiO_2 NPs and **b** TiO_2/PEG PNC

where new bands appear due to the presence of PEG. A strong peak around 1099 cm^{-1} attributable to C–C and C–O stretching vibrations. A sharp peak at 2872 cm^{-1} is also observed, corresponding to C–H stretching vibration; while the peak 3862 cm^{-1} in TiO_2 NPs for O–H disappears. This change confirms the chemically adsorption of PEG onto TiO_2 [28, 31, 32].

Thermal analysis

Figure 5 shows that PEG/TiO_2 PNC had an approximate two endothermic peak at ~ 60 °C and 144 °C with initial weight loss 2.5% attribute to the evaporation of absorbed water and ethanol [28]. Started from 280 °C till 539 °C, three endothermic peaks with total weight loss 51% are attributed to

Table 1 Porosity and pore parameters for TiO_2/PEG PNC

Sample	Pore size parameters			
	Average pore diameter (nm)	Porosity (%)	Bulk density (g/mL)	Apparent density (g/mL)
TiO_2/PEGPNC	257.1	32.78	0.8405	1.2503

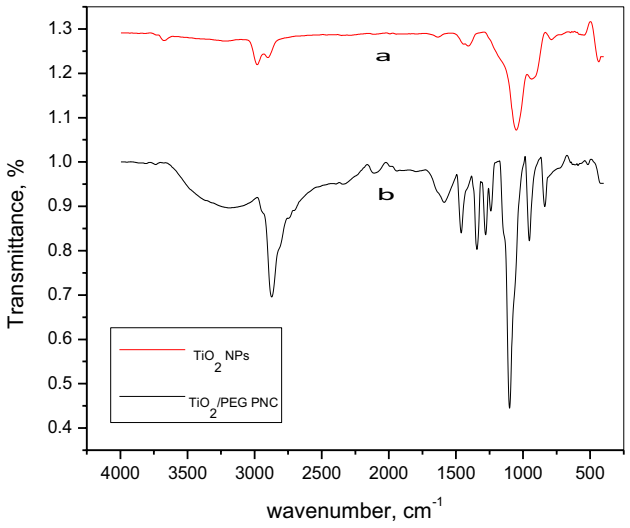

Fig. 4 FT-IR spectra for: (a) TiO_2 NPs, and (b) TiO_2/PEG PNC

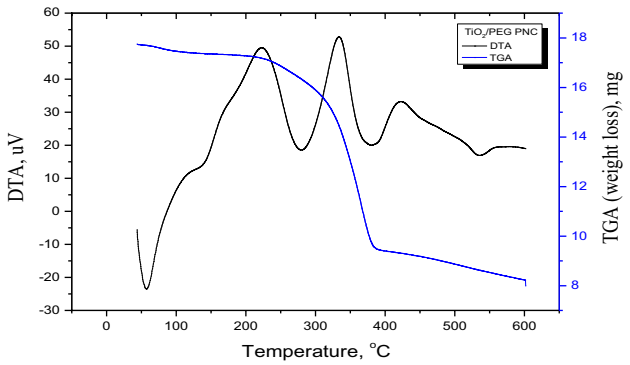

Fig. 5 TGA and DTA for the synthesized TiO_2/PEG PNC

organic matter degradation of PEG in TiO_2/PEG PNC [28, 31].

X-ray diffraction (XRD)

The result of XRD analysis of TiO_2/PEG PNC is represented in Fig. 6 and listed in Table 2. The crystallite structure of the nanocomposite is clarified through the intensity of

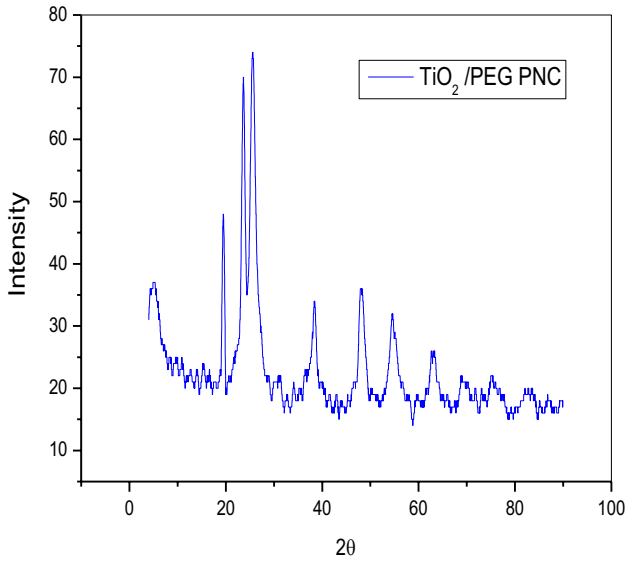

Fig. 6 XRD profiles of the TiO_2/PEG PNC

Table 2 XRD results of TiO_2/PEG PNC

Samples	XRD results		
	2θ	d-spacing (Å)	FWHM (deg)
TiO_2/PEG PNC	25.56	3.48	1.12
	23.62	3.76	0.73
	19.49	4.55	0.54

XRD peaks while the broad diffraction peaks indicate very small size crystallite For TiO_2/PEG PNC. The diffraction angle, 2θ = 25.5 [35] confirms TiO_2 anatase structure, while 2θ = 23.62, 19.49 confirms crystalline phase of PEG [24].

Sorption studies

The effect of pH

Figure 7a shows the effect of pH on the amount adsorbed (q_e) of ^{134}Cs and ^{60}Co radionuclides, different experiments were performed in the pH range 1–8. The sorption of both radionuclides is pH-dependent. The amount adsorbed of ^{134}Cs and ^{60}Co increase with increasing pH. At higher pH values, $[H^+]$ is low and the negative charge on the surface of the composite will increase enhancement the attraction forces among the surface of the composite and radionuclides increase, so the amount adsorbed of the radionuclides will increase. At lower pH values, the concentration of $[H^+]$ is high and competes the sorption of Cs and Co radionuclides on the surface of the composite and so decrease the amount adsorbed of these radionuclides [33].

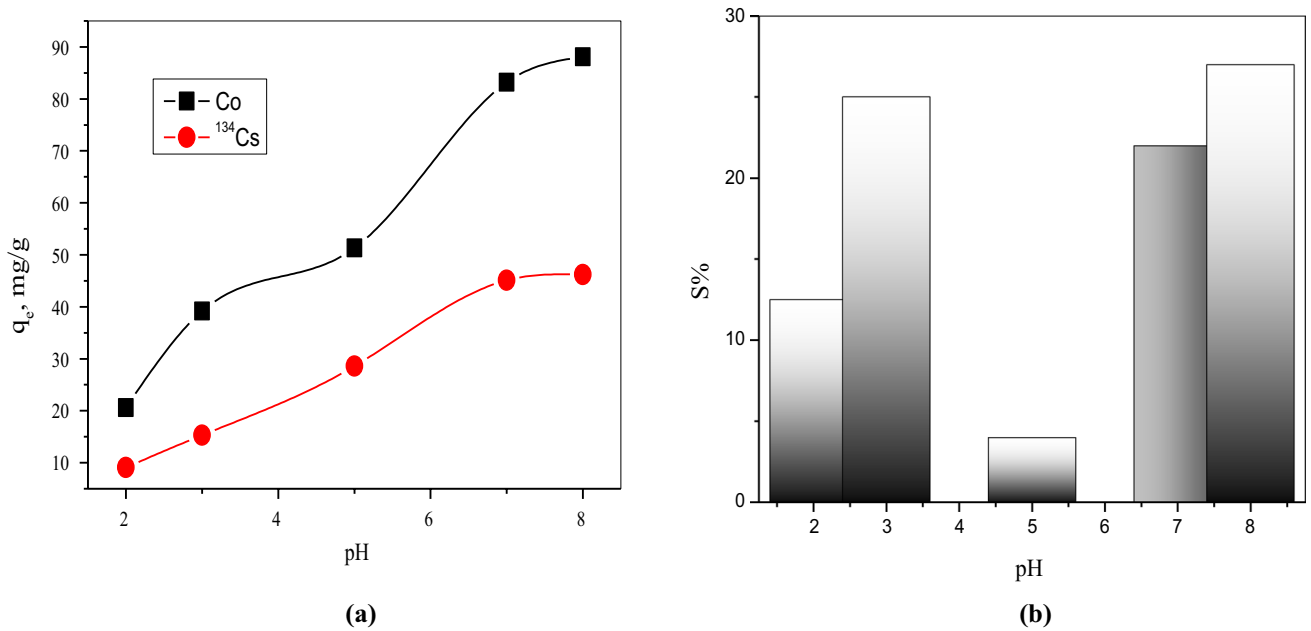

Fig. 7 **a** Effect of pH on the amount of adsorbed of ^{134}Cs, ^{60}Co on TiO_2/PEG PNC at room temperature and **b** stability of prepared TiO_2/PEG PNC powder in different pH

The speciation diagram of Cs^+ and Co^{+2} ions at different pH values in aqueous solution is shown in Fig. 8 using Hydra/Medusa chemical equilibrium software [34]. As pH increases, hydrolysis precipitation most probably would start due to the formation of various hydro complexes in aqueous solution [35].

At initial metal ions concentration, 50 mg L^{-1}, room temperature and different pH values (1–12). From Fig. 8a it is clear that the monovalent cesium (Cs^+) is the dominant species at all pH ranges. It is obvious that in Fig. 8b, the divalent species, Co^{2+}, is the dominant cobalt species at pH below 8, at the pH values > 8, the cobalt ion was precipitated as $Co(OH)_2$. So, the removal of cobalt below the

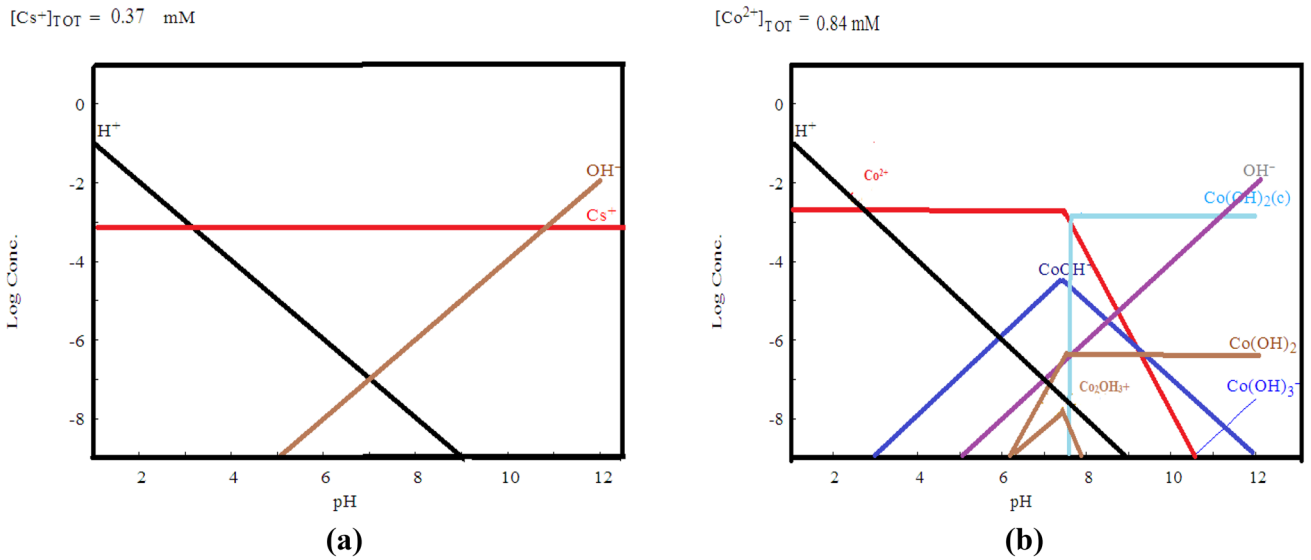

Fig. 8 Speciation of: **a** cesium and **b** cobalt ions at different pH and room temperature

pH < 8 is due to the sorption process but at a higher value of pH the hydrolysis of Co^{2+} [35], leading to the formation of $[CoOH]^+$ and $Co(OH)_2$, therefore, the precipitation process is the predominant mechanism at the higher pH values. So all the sorption experiments were carried out at pH 5 [35]. The result of chemical stability tests is shown in Fig. 7b. The prepared powder material was highly stable at pH 5 with weight loss of about 4%, and it witnessed considerable weight loss of 22, 25 and 27% at pH values 3, 7 and 8, respectively. In light of these findings, further experiments were performed in a solution of pH 5 to avoid any possible hydroxide precipitation and also ensure usage of the material in its most stable state.

The pH- distribution coefficient relation is shown in Table 3. The results obtained showed that K_d is pH-dependent. As the pH increases, k_d will increase for both radionuclides confirming the increase in amount sorbed of radionuclides as the pH increase.

Table 3 Distribution coefficients (K_d) of ^{134}Cs and ^{60}Co radionuclides sorbed by TiO_2/PEG PNC at different pH

pH	K_d (ml/g)	
	^{134}Cs	^{60}Co
2	20.02	51.89
3	36.13	128.95
5	80.11	210.78
7	164.29	990.27
8	171.75	1480.67

Effect of shaking time& temperature

The effect of shaking time on the sorption behavior of the studied radionuclides at temperatures 25 °C, 40 °C, and 60 °C is represented in Fig. 9. A certain weight (0.05 g) of the prepared nanocomposite and optimum pH 5. The results indicated that the sorption process was fast and equilibrium was reached within 30 min sorbents. The rapid radionuclides sorption onto TiO_2/PEG PNC sorbents can be explained by the availability of active sites on sorbent surfaces. The percent uptake was found to be 45.3, 52.5 and 58.1% for Cs^+ ions, and 83.3, 87.3 and 94.5% for ^{60}Co respectively. The amounts sorbed of ^{134}Cs radionuclide at equilibrium is 22.65, 26.25 and 29.05 mg g^{-1} at 25 °C, 40 °C and 60 °C respectively while the sorbed amounts of ^{60}Co radionuclide at equilibrium is 41.65, 43.75 and 47.25 mg g^{-1} at 25 °C, 40 °C and 60 °C respectively.

Sorption kinetics modeling

Kinetic models are used to determine the rate of sorption reaction and to investigate the mechanism of the sorption process.

The pseudo-first-order model was studied by applying the Non-linear pseudo-first- order Eq. (2) [36]:

$$q_t = q_e\left(1 - e^{-k_1 t}\right) \quad (2)$$

where q_e (mg g^{-1}), and q_t (mg g^{-1}), are the quantities of metal ion sorbed at equilibrium and at time t, respectively, and k_1 (min^{-1}), is the rate constant of the first-order equation.

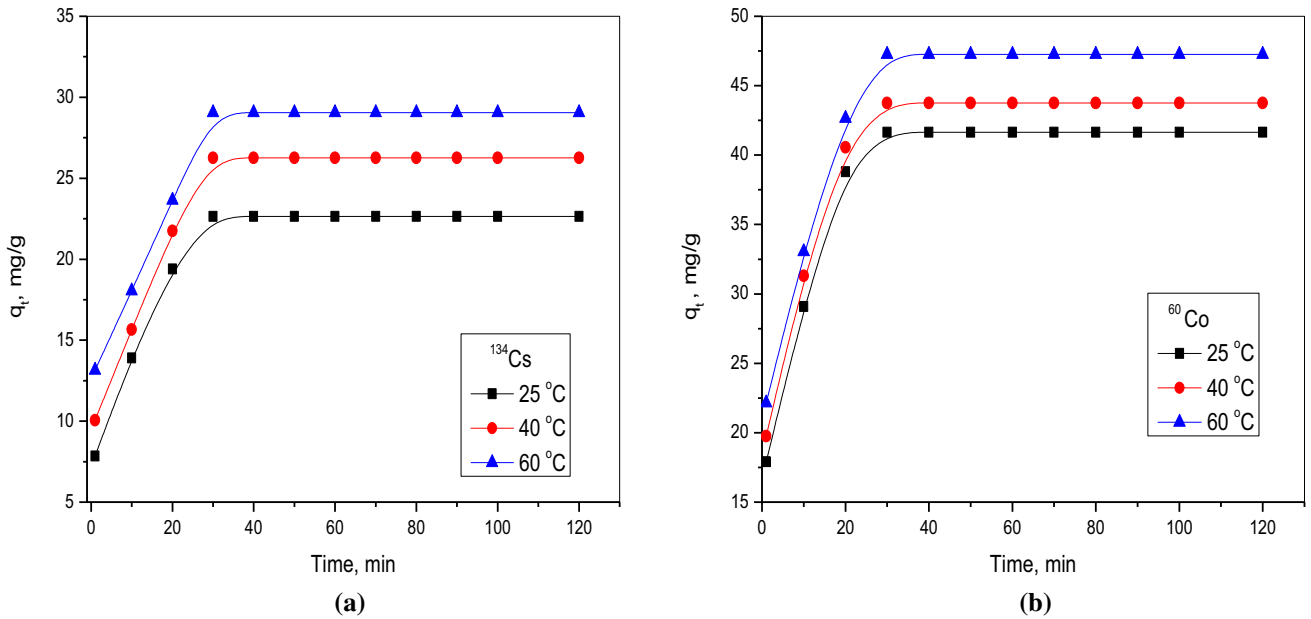

Fig. 9 Effect of contact time on the amount sorbed of **a** ^{134}Cs and **b** ^{60}Co onto TiO_2/PEG PNC at different temperatures, pH 5 and V/m = 200 mL/g

The pseudo-second-order non –linear equation is expressed as [36]:

$$q_t = \frac{k_2 q_e^2 t}{1 + k_2 q_e t} \quad (3)$$

where k_2 is a rate constant of the second-order model (g/mg. min). Figure 10 illustrates the fitting of the relation and the value of k_2 and q_e were determined and listed in Table 4. The pseudo-second-order equation is used with the assumption that the interaction between the adsorbate and adsorbent material is due to the chemisorption process.

Figure 10 expressing the relation fitting. Table 4 illustrated the values of q_e, k_1, k_2 and the correlation coefficient (R^2) of both radionuclides at three different temperatures. The values of the calculated capacity of the sorbed radionuclides at equilibrium q_e (cal.) must be in identity with the values of the experimental data q_e (exp.).

The values of q_e (cal.) are commensurate with the results of q_e (exp.) for both pseudo-first and pseudo- second- order. But, the high values of R^2 for pseudo-second-order elucidate that the sorption of ^{60}Co and ^{134}Cs radionuclides on TiO_2/PEG obeys pseudo-second-order kinetics. This fact shows that the pseudo-second-order model is the predominant model and the sorption process can be controlled by the chemical sorption process.

Equilibrium isotherm studies

The adsorption isotherm describes the relationship between the amount of sorbate on the sorbent at equilibrium, q_e, and the concentration of dissolved sorbate in the liquid, C_e Fig. 11 shows the plots between the amount of ^{134}Cs and

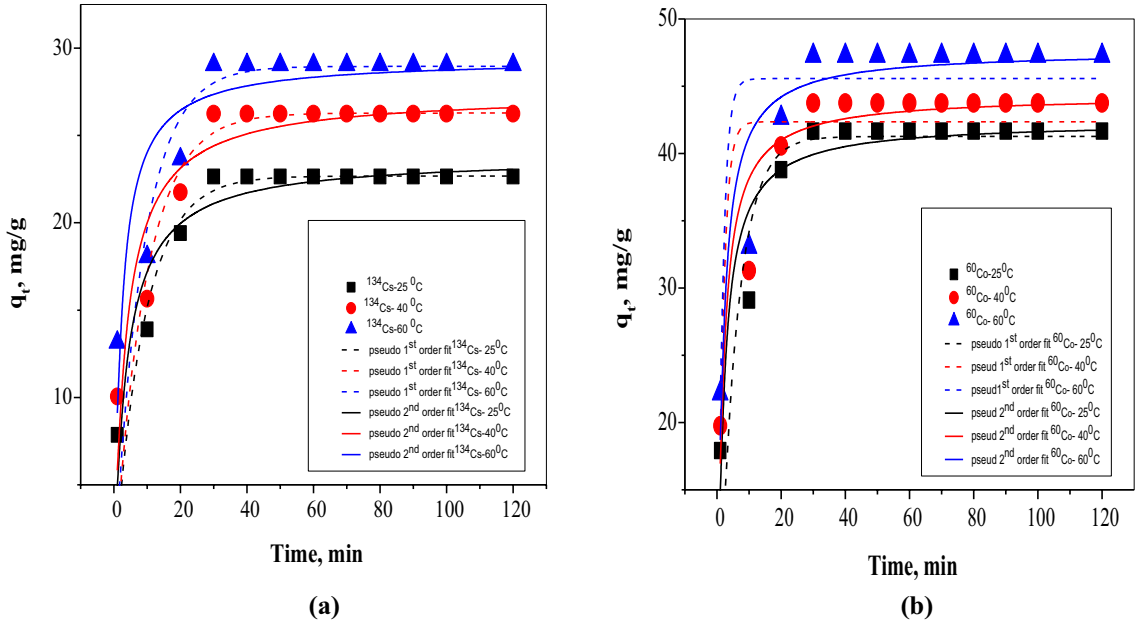

Fig. 10 Non-linear form fitting of pseudo-first order and pseudo-second order plots for the sorption of **a** ^{134}Cs and **b** ^{60}Co radionuclides onto TiO_2/PEG PNC at different temperatures

Table 4 Calculated parameters of the studied kinetic models for adsorption of ^{60}Co and ^{134}Cs onto TiO_2/PEG PNC

Radionuclide	Temperature (°C)	First-order kinetic parameters			$q_{e(exp)}$ mg/g)	Second-order kinetic parameters		
		k_1 (min^{-1})	q_e (cal.) (mg/g)	R^2		k_2 ($\times 10^{-3}$) (g/mg min)	q_e(cal.) (mg/g)	R^2
^{134}Cs	25	0.1049 ± 0.02	22.67526 ± 0.6384	0.8529	22.65 ± 0.33	0.01099 ± 0.0033	23.78652 ± 0.73825	0.89402
	40	0.10523 ± 0.02	26.28254 ± 0.87304	0.7882	26.25 ± 0.37	0.00984 ± 0.0035	27.4166 ± 0.9976	0.84426
	60	0.11436 ± 0.03	28.95577 ± 1.15955	0.6166	29.025 ± 0.39	0.01531 ± 0.0060	29.38326 ± 1.02265	0.76869
^{60}Co	25	0.17702 ± 0.05148	41.27 ± 1.29	0.7165	41.65 ± 1.21	0.01283 ± 0.00322	42.378 ± 0.9152	0.89219
	40	0.60763 ± 0.16473	42.358 ± 1.135	0.7457	43.75 ± 1.27	0.01398 ± 0.0034	44.30962 ± 0.90048	0.8907
	60	0.65071 ± 0.1853	45.56 ± 1.313	0.6994	47.25 ± 1.29	0.01357 ± 0.0037	47.62535 ± 1.0883	0.85676

^{60}Co radionuclides sorbed at equilibrium q_e, onto the papered TiO_2/PEG PNC and the initial metal ion concentrations C_o. The concentration of metal ions ranges 50–300 mg/L. From the Figure, it is observed that the amount sorbed of each radionuclide was increased with the increase of the initial concentration of the metal ions and temperature.

Langmuir and Freundlichisotherm models

The non-linear form of the Langmuir model can be expressed as the following [37]:

$$q_e = \frac{q_m b\, C_e}{1 + bC_e} \tag{4}$$

where q_m is the monolayer sorption capacity (mg g^{-1}), b is the constant related to the free energy of sorption (b α $e^{-\Delta G/RT}$) and Ce is the equilibrium metal ion concentration.

Also, the non-linear form of the Freundlich model can be expressed in Eq. (5) as the following [37]

$$q_e = k_f C_e^{1/n} \tag{5}$$

where, k_f is the Freundlich adsorption capacity coefficient (mg g^{-1}), 1/n is the adsorption intensity

Figure 12 represents non -linear form fitting of Langmuir isotherm and Freundlich models of ^{134}Cs and 60Co radionuclides sorption onto TiO_2/PEG PNC. On the basis of the parameters obtained from the Langmuir model (Table 5), the maximum sorption capacities of TiO_2/PEG PNC towards ^{134}Cs and ^{60}Co were calculated to be 163.28 ± 10.98, and 330.16 ± 41.60 mg g^{-1}, respectively at 25 °C. The sorption capacity of ^{134}Cs and ^{60}Co onto TiO_2/PEG PNC and the energy of sorption increased with temperature. The available active sites of TiO_2/PEG PNC increase as the temperature is raised, consequently the sorption capacity will increase.

Also, the numerical of $1/n < 1$ suggested that TiO_2/PEG PNC sorption reactions towards ^{134}Cs and ^{60}Co are favorable.

From the tabulated parameters, comparing the correlation coefficients of Langmuir isotherm model ($R^2 \geq 0.981$ for ^{134}Cs and $R^2 \geq 0.957$ for ^{60}Co radionuclide) with the correlation coefficients of Freundlich isotherm model ($R^2 \geq 0.98$ for ^{134}Cs and $R^2 \geq 0.98$ for ^{60}Co radionuclide), indicating that the Freundlich isotherm model is more applicable.

Temkin model:

Temkin isotherm linear form is given by Eq. (6) [38].

$$q_e = RT \ln K_T + RT/b\, C_e \tag{6}$$

where, K_T is the equilibrium binding constant (L mol^{-1}), the adsorption heat is (b), Fig. 13 represents Temkin isotherm plot. Table 6 shows the values of parameters and $R^2 \geq 0.96$ for ^{134}Cs and ≥ 0.92 for ^{60}Co.

Effect of metal-ion Interference

The sorption interference of specific ions on TiO_2/PEG PNC was studied. The sorption mixture of Na (I), Sr (II) and Fe

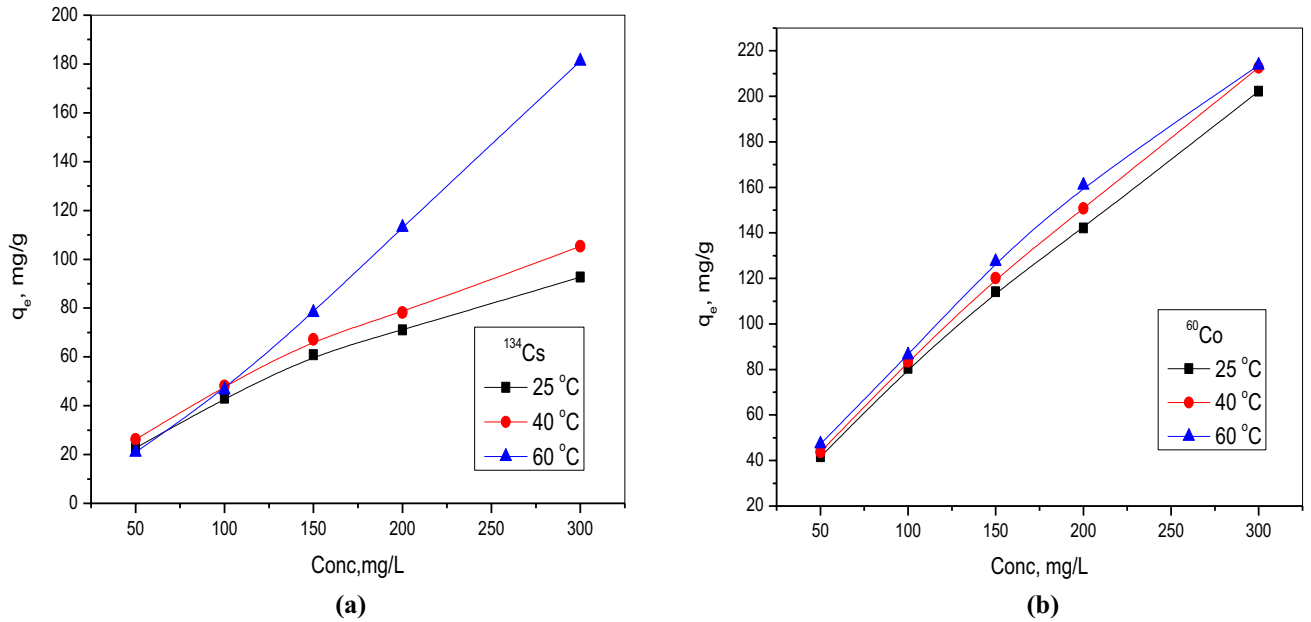

Fig. 11 Effect of metal ion concentrations on the amount sorbed of **a** ^{134}Cs and **b** ^{60}Co onto TiO_2/PEG PNC at pH 5, different temperatures, and V/m = 200 mL/g

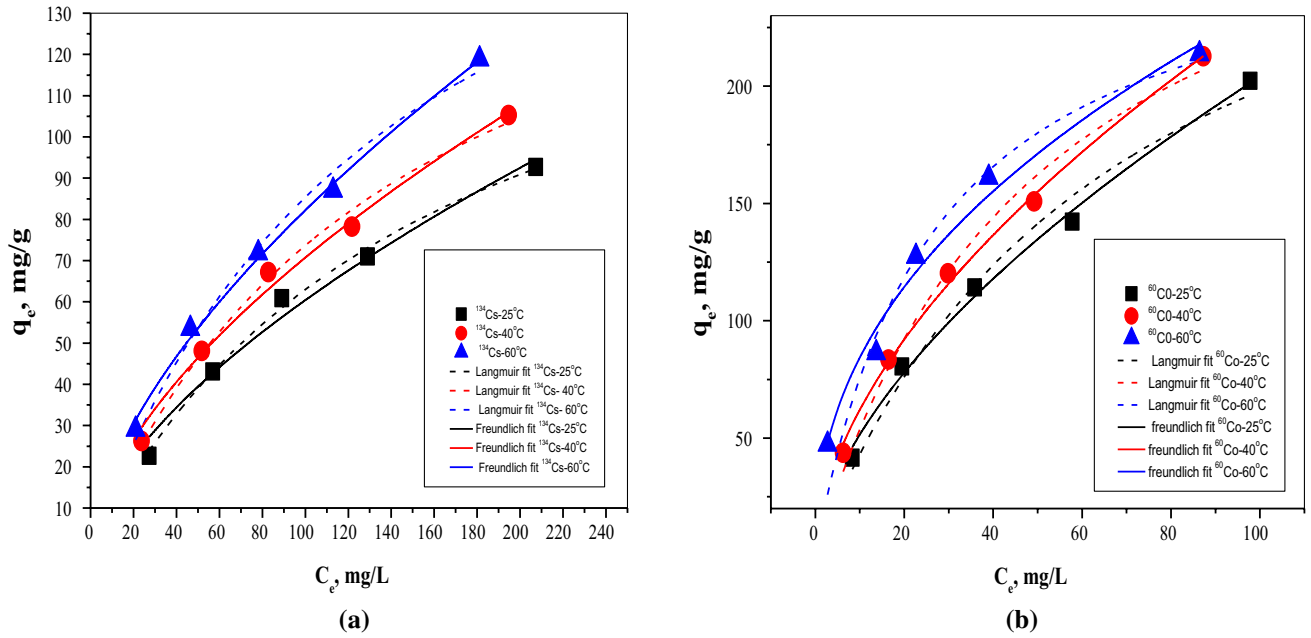

Fig. 12 Non-linear form fitting of Langmuir isotherm and Freundlich models of ^{134}Cs and ^{60}Co radionuclides sorption onto TiO_2/PEG PNC at different temperatures

Table 5 The values of parameters of Langmuir and Freundlich isotherm models for adsorption ions onto TiO_2/PEG PNC:

Metal ion	Temperature (°C)	Langmuir isotherm model			Freundlich isotherm model		
		$Q°$ (mg/g)	B (L/mg)	R^2	K_F(mg/g)	n	R^2
^{134}Cs	25	163.28742 ± 10.98998	0.00627 ± 7.62406E-4	0.9946	3.56131 ± 0.93513	1.62666 ± 0.1433	0.98
	40	180.76351 ± 15.5883	0.00688 ± 0.00108	0.9908	4.31702 ± 0.80847	1.64698 ± 0.1061	0.98
	60	207.83712 ± 22.50746	0.00697 ± 0.00135	0.9871	4.80804 ± 0.54776	1.62199 ± 0.0634	0.99
^{60}Co	25	330.16995 ± 41.60667	0.01497 ± 0.00356	0.9805	12.98732 ± 1.5734	1.67238 ± 0.0824	0.99
	40	328.34516 ± 34.84246	0.01955 ± 0.00413	0.9830	16.74114 ± 1.37129	1.75795 ± 0.063	0.99
	60	275.25992 ± 31.31084	0.0378 ± 0.01064	0.9576	30.6344 ± 4.2989	2.27373 ± 0.188	0.98

(III) were studied.; Contact time was 2 h with 0.05 g of sorbent dosage. It was shown that the presence of the monovalent, divalent and trivalent ions greatly affect the sorption of both ^{134}Cs and ^{60}Co radionuclides. The sorption capacities of TiO_2/PEG PNC towards ^{134}Cs and ^{60}Co increase in the order the ^{60} Co > ^{134}Cs. In presence of 50 mg L^{-1} of Sr (II), the amount sorbed from 83.3 to 9.5 mg g^{-1} and from 45.3 to 1.9 mg g^{-1} for ^{60}Co and ^{134}Cs, respectively. This might be due to the influence of ionic potential and ionic radius [39]. Figure 14 represents the metal-ion interfering effect on ^{134}Cs and ^{60}Co radionuclides onto TiO_2/PEG PNC.

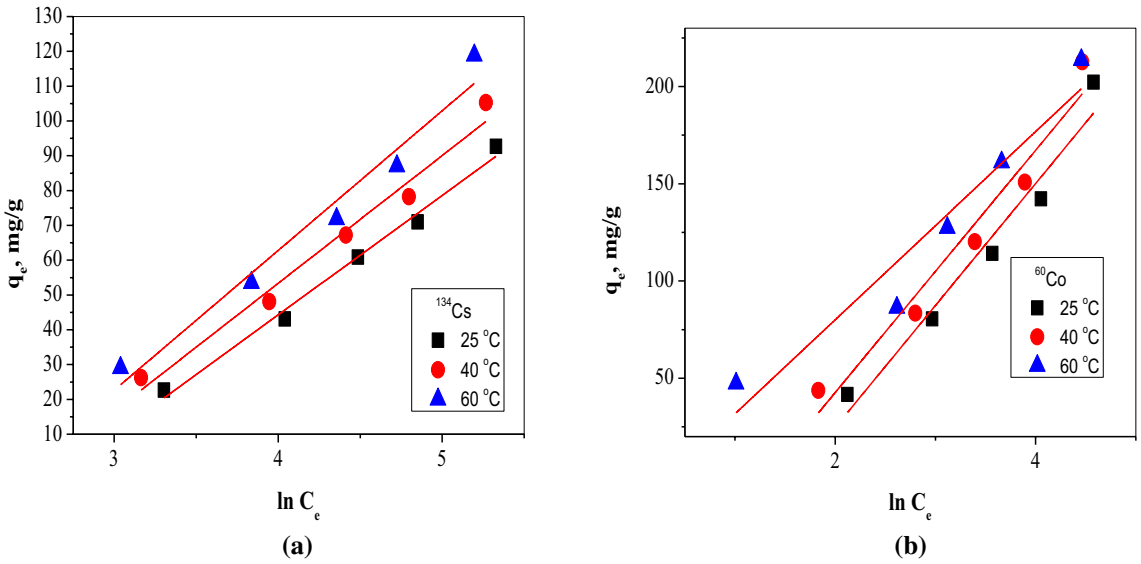

Fig. 13 Temkin isotherm plots of ^{134}Cs and ^{60}Co radionuclides sorption onto TiO_2/PEG PNC at different temperatures, pH 5 and V/m = 200 mL/g

Table 6 The values of parameters of the Temkin isotherm model for ^{134} Cs and ^{60}Co radionuclides sorption onto TiO_2/PEG PNC:

Metal ion	Temperature (°C)	Temkin isotherm model		
		b	K_T(L mol^{-1})	R^2
^{134}Cs	25	72.23 ± 1.44	0.066 ± 0.0005	0.99
	40	68.639 ± 1.56	0.078 ± 0.0007	0.97
	60	68.975 ± 1.89	0.087 ± 0.0008	0.96
^{60}Co	25	39.503 ± 0.91	0.201 ± 0.001	0.95
	40	40.444 ± 0.95	0.268 ± 0.004	0.95
	60	57.217 ± 0.98	0.707 ± 0.008	0.92

Thermodynamic studies

The sign of the free energy, ($\Delta G°$ kJ/mol, determines the favorability of the sorption process. $\Delta G°$ is calculated with Eq. (7) aid.

$$\Delta G^{\circ} = -RT \ln K_c \quad (7)$$

where, the universal gas constant is R (8.314 J K^{-1} mol^{-1}), Temperature is T (K), and the equilibrium constant of the sorption process is K_c. The values of other thermodynamic parameters such as $\Delta H°$ (kJ/mol (and $\Delta S°$ (J/mol K) have been calculated using the following Eq. (8).

$$\ln K_C = \Delta S^{\circ}/R - \Delta H^{\circ}/RT \quad (8)$$

Figure 15 shows the plot between ln K_c and 1/T. The values of $\Delta H°$ are positive emphasize an endothermic sorption reaction of ^{134}Cs and ^{60}Co radionuclides onto TiO_2/PEG PNC as shown in Table 7. Also, the positive values of $\Delta S°$ indicate an increase in the randomness at the sorbent/radionuclides interface and a good affinity of sorbents towards the radionuclide [40].

Conclusion

TiO_2/PEG PNC was successfully prepared by wet-chemical method and physic-chemically characterized by some analytical techniques such as (TEM), (FTIR), (XRD), (DTA-TGA), particle size distribution, and pore size analysis. TiO_2/PEG PNC used for sorption of ^{134}Cs and ^{60}Co radionuclides from aqueous solutions at pH 5. The equilibrium was reached after about 30 min. Pseudo second order model is applicable with

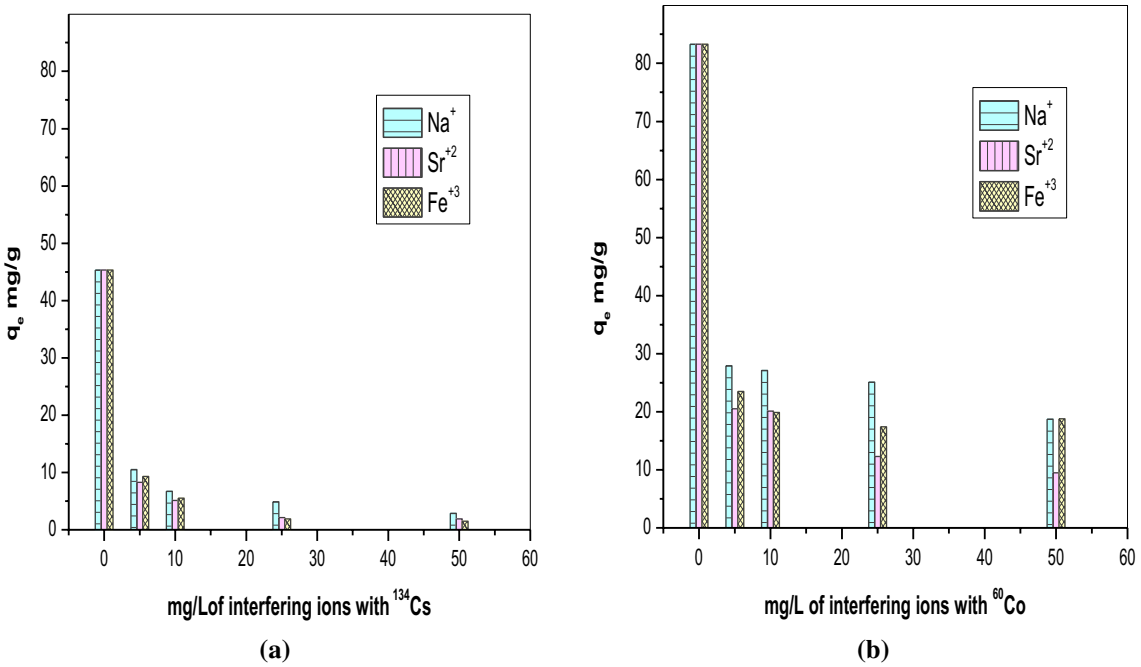

Fig. 14 Metal-ion interfering effect on **a** ^{134}Cs and **b** ^{60}Co radionuclides sorption onto TiO_2/PEG PNC

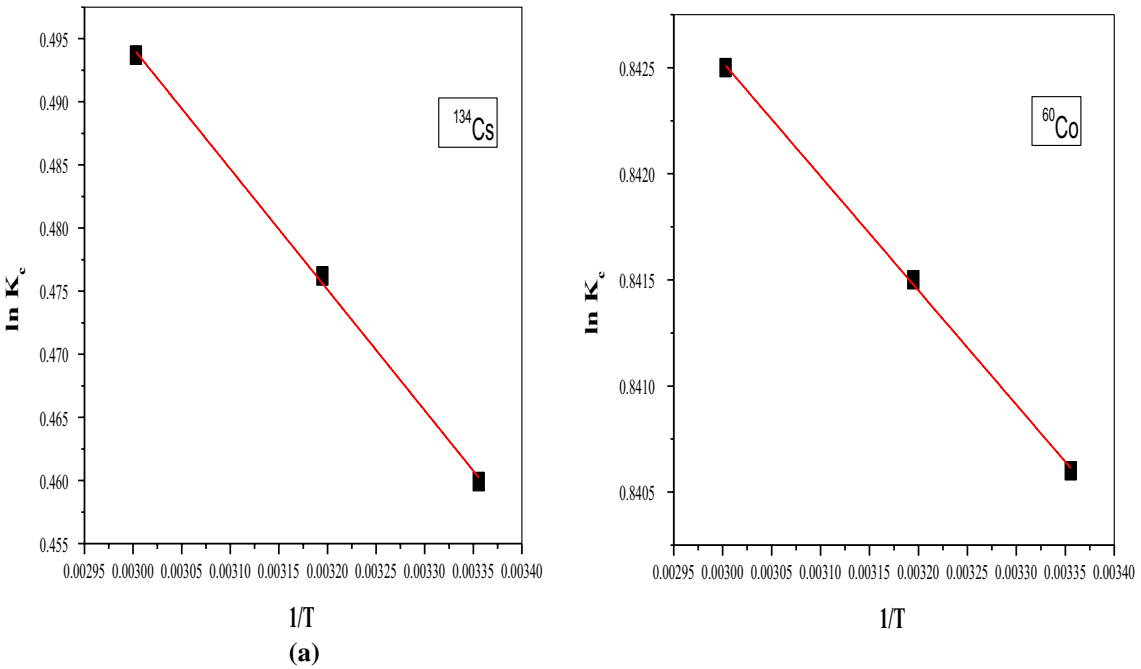

Fig. 15 Thermodynamic plot for the sorption of **a** ^{134}Cs and **b** ^{60}Co radionuclides onto TiO_2/PEG PNC

Table 7 Thermodynamic parameters for the sorption of ^{134}Cs and ^{60}Co radionuclides onto TiO_2/PEG PNC:

Radionuclides	ΔG°, J/mol			ΔH° (J/mol)	ΔS°, (J/mol K)
	298 K	313 K	333 K		
^{134}Cs	−1137 ± 22.1	−1237.1 ± 20.6	−1364 ± 23.78	794.17 ± 10.3	6.484 ± 0.9
^{134}Co	−2079 ± 24.4	−2186 ± 30.7	−2328 ± 29.9	44.66 ± 3.2	7.12 ± 1.6

the sorption reaction mechanism. The monolayer capacities (at pH 5 and 25 °C) of ^{134}Cs and ^{60}Co radionuclides on TiO_2/PEG PNC were found to be 163.28 ± 10.98, and 330.16 ± 41.60 mg g^{-1}, respectively. The thermodynamic studies explain favorability and endothermic nature of the sorption process. Therefore, TiO_2/PEG PNC could be used as an efficient sorbent for ^{134}Cs and ^{60}Co radionuclides. The study demonstrates that interference with co-metals is an important factor for consideration in TiO_2/PEG PNC sorption application.

References

1. Hengleir A (1989) Small-particle research: physicochemical properties of extremely small colloidal metal and semiconductor particles. Chem Rev 89:1861. https://doi.org/10.1021/cr00098a010
2. Khin MM, Sreekumaran Nair A, Jagadeesh Babu V, Murugan R, Ramakrishnam S (2012) A review on nanomaterials for environmental remediation. Energy Environ Sci 5:8075–8109. https://doi.org/10.1039/C2EE21818F
3. Niederberger M (2007) Nonaqueous sol–gel routes to metal oxide nanoparticles. Acc Chem Res 40:793–800. https://doi.org/10.1021/ar600035e
4. Liang P, Qin Y, Hu B, Li C, Peng T, Jiang Z (2000) Study of the adsorption behavior of heavy metal ions on nanometer-size titanium dioxide with ICP-AES. Fresenius J Anal Chem 368:638–640. https://doi.org/10.1007/s002160000546
5. Liang P, Hu B, Jiang Z, Qin Y, Peng T (2001) Nanometer-sized titanium dioxide micro-column on-line preconcentration of La, Y, Yb, Eu, Dy and their determination by inductively coupled plasma atomic emission spectrometry. J Anal Atom Spectrom 16:863–866. https://doi.org/10.1039/b104050m
6. Pan B, Pan B, Zhang W, Lv L, Zhang Q, Zheng S (2009) Development of polymeric and polymer-based hybrid adsorbents for pollutants removal from waters. Chem Eng J 151:19–29. https://doi.org/10.1016/j.cej.2009.02.036
7. Hua M, Zhang S, Pan B, Zhang W, Lv L, Zhang Q (2012) Heavy metal removal from water/wastewater by nanosized metal oxides: a review. J Hazard Mater 211:317–331. https://doi.org/10.1016/j.jhazmat.2011.10.016
8. Zainab M, Jeefferie AR, Masrom AK, Rosli ZM (2012) Effect of PEG molecular weight on the TiO_2 particle structure and TiO_2 thin films properties. Adv Mater Res 364:76–80. https://doi.org/10.4028/www.scientific.net/AMR.364.76
9. Santos ÁA, Acevedo-Peña P, Córdoba EM (2012) Enhanced photocatalytic activity of TiO_2 films by modification with polyethylene glycol. Quim Nova 35:1931–1935. https://doi.org/10.1590/S0100-40422012001000008
10. Wang S-H, Wang K-H, Dai Y-M, Jehng J-M (2013) Water effect on the surface morphology of TiO_2 thin film modified by polyethylene glycol. Appl Surf Sci 264:470–475. https://doi.org/10.1016/j.apsusc.2012.10.046
11. Chang H, Jo EH, Jang HD, Kim TO (2013) Synthesis of PEG-modified TiO_2–$InVO_4$ nanoparticles via combustion method and photocatalytic degradation of methylene blue. Mater Lett 92:202–205. https://doi.org/10.1016/j.matlet.2012.11.006
12. Trapalis C, Keivanidis CP, Kordas G, Zaharescu M, Crisan M, Szatvanyi A, Gartner M (2003) TiO_2 (Fe^{3+}) nanostructured thin films with antibacterial properties. Thin Solid Films 431:186–190. https://doi.org/10.1016/S0040-6090(03)00331-6
13. Ngwenya N, Chirwa EMN (2010) Single and binary component sorption of the fission products Sr^{2+}, Cs^{+} and Co^{2+} from aqueous solutions onto sulphate reducing bacteria Miner. Miner Eng 23:463–470. https://doi.org/10.1016/j.mineng.2009.11.006
14. Ma B, Oh S, Shin WS, Choi S-J (2011) Removal of Co^{2+}, Sr^{2+} and Cs^{+} from aqueous solution by phosphate-modified montmorillonite (PMM). Desalination https://doi.org/10.1016/j.desal.2011.03.072
15. El-Zakla T, Yakout SM, Rizk MA, Lasheen YF, Gad HMH (2011) Removal of cobalt-60 and caesium-134 ions from contaminated solutions by sorption using activated carbon. Adsorpt Sci Technol J. 29(3):331–344. https://doi.org/10.1260/0263-6174.29.3.331
16. Horyna J, Dlouhy Z (1988) A study on the sorption properties of selected clays. Jaderna Energie 34(8):300–302
17. Aksoyoglu S (1990) Cesium sorption on mylonite. J Radioanal Nucl Chem Art 140(2):301–313. https://doi.org/10.1007/BF02039502
18. El-Dessouky MM (1990) Radioactive decontamination of drinking water and treatment of low level waste using some local natural materials. J Environ Sci 1:145–153
19. Abou-Jamous JKh (1992) Radioactive waste treatment using natural syrian bentonite. J Radioanal Nucl Chem Art 162(2):325–338. https://doi.org/10.1007/BF02035393
20. El-Naggar IM, El-Absy MA, Abdel Hamid MM, Aly HF (1993) Sorption behaviour of uranium and thorium on cryptomelane-type hydrous manganese dioxide from aqueous solution. Solvent Extr Ion Exch 11(3):521–540. https://doi.org/10.1080/07366299308918171
21. Dandautiya Rahul, Singh Ajit Pratap, Kundu Sanghamitra (2018) Impact assessment of fly ash on ground water quality: an experimental study using batch leaching tests. Waste Manag Res J. 36(7):624–634. https://doi.org/10.1177/0734242X18775484
22. Spence RD, Gilliam TM, Osborne SC, Francis CL, Trotter DR (1993) Evaluation of dry-solids blend material source for grouts containing 106-AN waste: final report. ORNL, TN (U.S.), Funding Organization: USDOE, Washington, DC (U.S), 267 p, Sep. https://doi.org/10.2172/10184762
23. ElRahman GA (2000) Immobilization studies of certain radioactive waste elements in ceramic or glass matices. M.Sc.thesis, Chemistry Department, Faculty of Science, Cairo University
24. Kang H, Li G (2011) Preparation and study of polyethylene glycol (PEG)/titanium dioxide (TiO_2) phase change materials. Adv Mater Res 284–286:214–218. https://doi.org/10.4028/www.scientific.net/AMR.284-286.214
25. El-gammal B, Shady SA (2006) Chromatographic separation of sodium, cobalt and europium on the particles of zirconium molybdate and zirconium silicate ion exchangers. Coll Surf A: Physicochem Eng Asp 287:132–138. https://doi.org/10.1016/j.colsurfa.2006.02.068
26. Behnam MA, Emami F, Sobhani Z, Dehghanian AR (2018) The application of titanium dioxide (TiO_2) nanoparticles in the photothermal therapy of melanoma cancer model. Iran J Basic Med Sci 21(11):1133–1139. https://doi.org/10.22038/IJBMS.2018.30284.7304
27. Motzkus C, Macé T, Vaslin-Reimann S, Ausset P, Maillé M (2013) Characterization of manufactured TiO2 nanoparticles. Nanosafe 2012: international conferences on safe production and use of nanomaterials. IOP Publ J Phy Conf 429:012012. https://doi.org/10.1088/1742-6596/429/1/012012
28. Yu K, Zhao J, Zhao X, Ding X, Zhu Y, Wang Z (2005) Self-assembly and oriented organization of shape controlled nanocrystalline TiO_2. Mater Lett 59:2676–2679. https://doi.org/10.1016/j.matlet.2005.04.017

29. Shaojing Bu, Jin Z, Liu X, Yang L, Cheng Z (2004) Fabrication of TiO_2 porous thin films using peg templates and chemistry of the process. Mater Chem Phys 88:273–279. https://doi.org/10.1016/j.matchemphys.2004.03.033
30. Fathima B, John M, Sharfudeen AF, Latheef A, Ambrose RV (2017) Synthesis and characterization of TiO_2 nanoparticles and investigation of antimicrobial activities against human pathogens. J Pharm Sci Res 9(9):1604–1608
31. León A, Reuquen P, Garín C, Segura R, Vargas P, Zapata P, Orihuela PA (2017) FTIR and Raman characterization of TiO_2 nanoparticles coated with polyethylene glycol as carrier for 2-methoxyestradiol. J Appl Sci 7:49. https://doi.org/10.3390/app7010049
32. Shi Q, Yua J, Liu T (2011) Preparation and performance of polyethylene glycol/titanium dioxide phase change materials. Adv Mater Res 183(185):2082–2085. https://doi.org/10.4028/www.scientific.net/AMR.183-185.2082
33. Kurniawan TA, Chan GYS, Lo WH, Babel S (2006) Comparisons of low-cost adsorbents for treating wastewaters laden with heavy metals. J Sci Total Environ 366:409–426. https://doi.org/10.1016/j.scitotenv.2005.10.001
34. Puigdomenech I (2013) Make equilibrium diagrams using sophisticated algorithms (MEDUSA). Inorganic Chemistry. Royal Institute of Technology, Stockholm Sweden. https://www.kemi.kth.se/medusa; https://sites.google.com/site/chemdiagr/
35. Dakroury GA, Abo-Zahra SF, Hassan HS, Fathy NA (2019) Utilization of silica-chitosan nanocomposite for removal of $^{152+154}$Eu radionuclide from aqueous solutions. J Radioanal Nuclear Chem. https://doi.org/10.1007/s10967-019-06951-6
36. Lin J, Wang L (2009) Comparison between linear and non-linear forms of pseudo-first-order and pseudo-second-order adsorption kinetic models for the removal of methylene blue by activated carbon. Front Environ Sci Eng China 3:320–324. https://doi.org/10.1007/s1783-009-0030-7
37. Mohammadi M, Ameri Shahrabi MJ, Sedighi M (2012) Comparative study of linearized and non-linearized modified Langmuir isotherm models on adsorption of asphaltene onto mineral surfaces. Surf Eng Appl Electrochem 48:234–243. https://doi.org/10.3103/S1068375512030088
38. Vijayaraghavan K, Padmesh TVN, Palanivelu K, Velan M (2006) Biosorption of nickel(II) ions onto *Sargassum wightii*: application of two-parameter and three-parameter isotherm models. J Hazard Mater 133(1–3):304–308. https://doi.org/10.1016/j.jhazmat.2005.10.016
39. Sharma M, Choudhury D, Hazra S, Basu S (2017) Effective removal of metal ions from aqueous solution by mesoporous MnO_2 and TiO_2 monoliths: kinetic and equilibrium modeling. J Alloys and Comp 720:221–229. https://doi.org/10.1016/j.jallcom.2017.05.260
40. KarolinaWieszczyck KF, Wojciechowska I, Aksamitowski P (2020) Novel ionic liquid-modified polymers for highly effective adsorption of heavy metals ions. Sep Purif Technol 236:116313. https://doi.org/10.1016/j.seppur.2019.116313